# Alloying of Fe/Cr/Ni Thin Films by Ultrashort Pulsed Laser Irradiation Studied by Transmission Electron Microscopy

Koji Nakagawa<sup>1</sup>, Hiroto Seki<sup>1</sup>, Taiyoh Kawano<sup>1</sup>, Takashi Takahashi<sup>2</sup>, Keisuke Takabayashi<sup>2,3</sup>, Tsubasa Endo<sup>2</sup>, Eibon Tsuchiya<sup>2</sup>, Makoto Yamaguchi<sup>3</sup>, Tatsuya Okada<sup>1</sup>, Yohei Kobayashi <sup>2</sup>, and Takuro Tomita\*<sup>1</sup>

<sup>1</sup>Graduate School of Science and Technology for Innovation, Tokushima University, Japan

<sup>2</sup> Institute for Solid State Physics, University of Tokyo, Japan

<sup>3</sup>Graduate School of Engineering Science, Akita University, Japan

\*Corresponding author's e-mail: tomita@tokushima-u.ac.jp

The formation of ternary alloys induced by ultrashort pulsed laser irradiation was investigated. Thin films of Fe, Cr, and Ni were sequentially deposited onto a sapphire substrate. Laser irradiation was performed from the sapphire substrate side, with the focal point at the interface between the substrate and the metal layers. Energy-dispersive X-ray spectroscopy (EDS) analysis showed no significant difference between the samples irradiated by 300 fs laser and 10 ps laser. At a fluence of 0.03 J/cm², all three elements were mixed while the morphology of the metal films remained intact. As the laser fluence increased, the metal film morphology became increasingly disrupted. At 0.20 J/cm², the Cr and Ni layers were completely ablated. In contrast, annealing did not produce regions where the three elements were mixed. Instead, Fe and Ni were observed to have aggregated into droplet-like structures. Selected area electron diffraction (SAED) analysis suggested the presence of various oxides, binary alloys, and ternary alloy for both pulse durations.

DOI: 10.2961/jlmn.2025.03.2013

**Keywords:** thin films, laser-induced alloying, non-thermodynamics, quenching effect, binary alloy, ternary alloy

### 1. Introduction

In recent years, high-entropy alloys (HEAs) have attracted considerable attention in materials science [1-5]. Unlike conventional alloys, which typically consist of a primary element with additions of minor elements, HEAs are composed of five or more elements in approximately equal proportions, with no dominant component [6]. These alloys are known for their excellent biocompatibility and mechanical performance [7]. Traditionally, biomaterials have relied on expensive metals such as gold and titanium, while rare and costly metals are also widely used in the electronics industry. However, these resources are limited and their supply is subject to geopolitical and socioeconomic constraints. To address this issue, we aimed to develop HEAs with properties comparable to those of rare and expensive metals, using more abundant and accessible elements. The successful development of such alloys could significantly reduce manufacturing costs and promote progress in various industries. Despite their potential, fabricating HEAs poses several challenges, including elemental segregation and difficulty in precisely controlling composition ratios. Among the various synthesis techniques, selective laser melting (SLM), e.g., a laser-based additive manufacturing process, has emerged as a promising approach [8]. In recent years, continuous wave (CW) lasers have been commonly used in SLM. Compared to traditional casting, SLM provides cooling rates exceeding 107 K/s, which can suppress elemental segregation during alloy formation [9-10].

Ultrashort pulsed lasers, such as femtosecond lasers, have higher peak intensities than CW lasers. Due to their extremely short thermal diffusion lengths, they are expected to achieve even faster cooling, potentially exceeding 1013 K/s [11]. Even for alloy systems that are typically accessible through conventional thermal processing methods, ultrashort pulsed laser irradiation presents significant advantages owing to its exceptionally high cooling rates compared to techniques such as powder metallurgy and laser cladding. These rapid solidification conditions effectively suppress elemental segregation and surface oxidation, facilitating the formation of compositionally uniform and structurally refined alloys. Moreover, as the compositional complexity increases particularly in future studies involving multicomponent systems the control of segregation and oxidation becomes increasingly difficult. Under such conditions, the unique benefits of ultrashort pulse laser processing are expected to play an even more critical role in achieving high quality, metastable alloy phases.

However, reports on alloy fabrication using ultrashort pulsed lasers remain limited, and many aspects including the control of composition ratios and the relationship between laser parameters and resulting material properties are not yet fully understood. Our research group previously demonstrated the successful formation of a solid solution of Au and Ni by femtosecond laser irradiation [12]. Although Au and Ni typically mix at elevated temperatures (~810°C), they

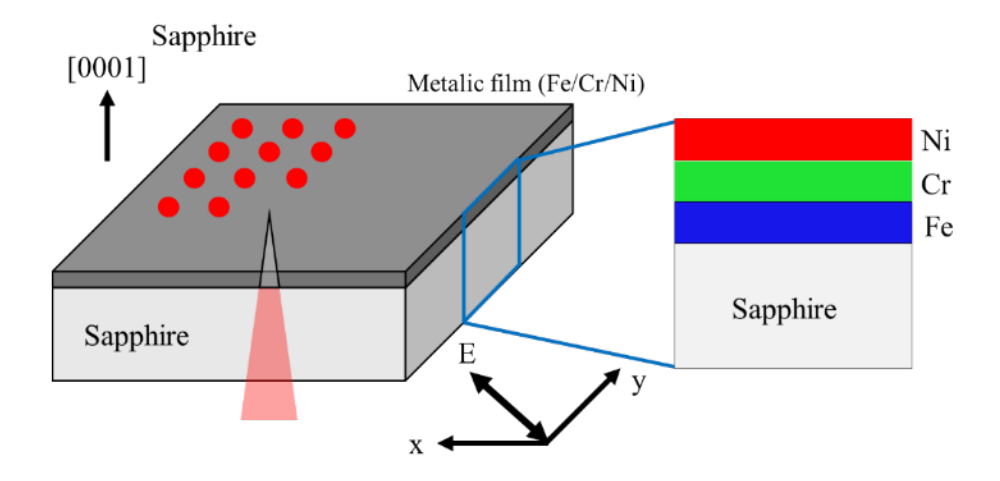


**Fig. 1** The laser irradiation was focused from the sapphire substrate side onto the interface between the sapphire substrate and the Fe layer. Laser irradiation was applied in the direction parallel to the [0001] crystallographic axis of the sapphire substrate. The electric field is oriented diagonally with respect to both the x- and y-axes.

tend to separate upon cooling, preventing solid solution formation. We attribute the stabilization of the Au–Ni solid solution at room temperature to the ultrafast heating and quenching induced by femtosecond laser pulses, which inhibit phase separation. In addition to Au–Ni alloys, laser irradiation of Sn and Cu has been reported to quench  $\delta$ -phase which is stable at high temperatures [13]. Conversely, a previous study involving laser irradiation of Fe, Cr, and Ni did not confirm ternary alloy formation, likely due to the oxidation of Ni during processing [14].

## 2. Experimental

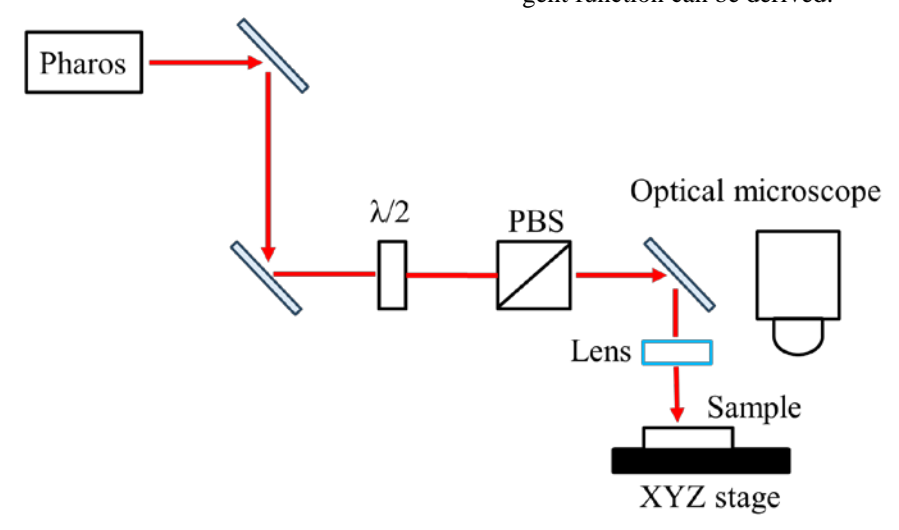
We used sapphire substrates as transparent materials. The sapphire substrates had a thickness of  $430\pm50\,\mu m$  and were cut into 10 mm  $\times$  10 mm pieces. As shown in Figure 1, thin films of Fe, Cr, and Ni, each with a thickness of 10 nm, were sequentially deposited onto the sapphire substrates. Fe, Cr, and Ni were all deposited by electron beam evaporation. The film thickness was measured using a quartz crystal unit, which also allowed for nm scale control of the deposition process through adjustments of the deposition rate and the use of a shutter.

Figure 2 shows the optical path of the laser processing. In this study, we used a laser with Yb:KGW crystal as the medium. The laser irradiation parameters were as follows: The wavelength was 1030 nm. The pulse duration was adjusted to either 10 ps or 300 fs. Laser irradiation was performed from the sapphire substrate side, with the beam focused on the interface between the Fe film and the substrate.

Figure 3 illustrates a schematic representation of the optical geometry used to focus the laser beam at the substrate film interface through a transparent substrate. Let  $\theta_I$  [rad] represent the angle of laser incidence in air,  $\theta_2$  [rad] the refracted angle within the substrate, Z [ $\mu$ m] the penetration depth required to focus on the interface after initially focusing on the surface,  $\Delta Z$  [ $\mu$ m] the deviation between Z and the actual focal point, d [ $\mu$ m] the total thickness of the substrate,  $n_1$  the refractive index of the incident medium, and  $n_2$  the refractive index of the substrate. According to Snell's law, the relationship between the incident and refracted angles is given by:

$$n_1 sin\theta_1 = n_2 sin\theta_2. \tag{1}$$

From the geometric relationship between Z, d, and the respective angles, the following expression using the tangent function can be derived:



**Fig.2** The laser beam is tuned using a half-wave plate and a polarizing beam splitter. Subsequently, irradiation marks were observed using an optical microscope.

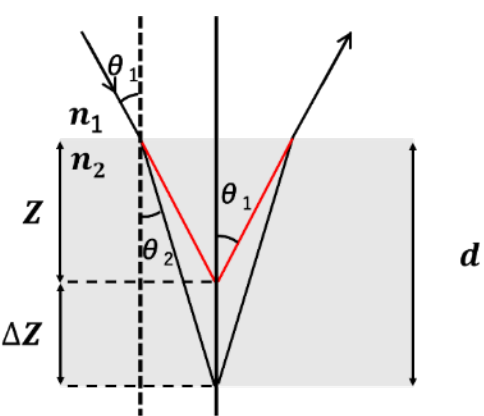


**Fig.3** After initially focusing on the substrate surface, the focal plane is adjusted to the bottom interface of the substrate and the Fe film by compensating for the substrate thickness and its refractive index.

$$Z tan \theta_1 = d tan \theta_2. \tag{2}$$

Given that  $\theta_1$  and  $\theta_2$  are infinitesimally small,

$$Z = d \frac{\sin \theta_2}{\sin \theta_1}.$$
 (3)

Accordingly, by substituting Eq. (1), the required penetration depth into the substrate after initial surface focusing can be expressed as follows:

$$Z = \frac{n_1}{n_2} d. (4)$$

By substituting the values  $n_1$ =1,  $n_2$ =1.7682, d=430  $\mu$ m into the above equation, the penetration depth Z is calculated to be 243  $\mu$ m. Accordingly, in order to focus the laser precisely at the interface between the bottom surface of the substrate and the Fe thin film, the focal plane must be translated approximately 243  $\mu$ m below the top surface of the substrate.

The repetition rate was 1 kHz, and 3000 pulses were applied to the same location. The fluence was varied from 0.02 J/cm² to 0.3 J/cm² in increments of 0.02 J/cm². Each irradiation condition was repeated twice, with a spot diameter of 82  $\mu m$ . To prevent interaction between irradiated areas, a minimum spacing of 200  $\mu m$  was maintained, as illustrated in Figure 4. For comparison, thermal annealing was conducted. The temperature was increased from room temperature to 1000 °C in 1 minute. After maintaining the

temperature at 1000 °C for 2 minutes, the sample was rapidly cooled by water quenching.

After laser irradiation, the samples were analyzed using transmission electron microscopy (TEM) to examine the effects of laser processing. For TEM observation, the samples were thinned to approximately 100 nm using a focused ion beam (FIB) system. Prior to FIB processing, a carbon protective layer was deposited on the sample surface to prevent ion beam damage. Following FIB processing, the sample was transferred onto a grid mesh using a micromanipulator. Energy-dispersive X-ray spectroscopy (EDS) was performed to investigate elemental mixing. In addition, selected-area electron diffraction (SAED) analysis was conducted to determine the crystallographic interplanar distance (d-value) of newly formed alloy phases.

Based on the obtained d-values, a crystallographic database software (CSManager) was used to search for potential candidate phases. These analyses allowed us to identify the products formed by laser irradiation.

#### 3. Result and discussion

Figure 5 shows a scanning transmission electron microscopy (STEM) bright-field image and a corresponding EDS elemental map of the sample prior to laser irradiation. The STEM image confirms that the metal films were uniformly deposited on the sapphire substrate. In the EDS maps, Fe, Cr, and Ni are visualized in blue, green, and red, respectively. Although slight intermixing of Cr and Ni is observed likely due to partial melting during deposition, the layered structure of the films remains largely intact.

Figure 6 shows EDS images of regions subjected to laser irradiation. The observed trends were consistent for both pulse durations (300 fs and 10 ps). At a peak fluence of 0.03 J/cm², the three elements were mixed within the irradiated region, while the overall morphology of the metallic film was well preserved. At a higher fluence of 0.06 J/cm², partial melting occurred. A bright region was observed, indicating apparent mixing of Fe, Cr, and Ni, along with localized damage to the film structure. When the peak fluence was further increased to 0.20 J/cm², a considerable amount of Fe remained at the bottom of the irradiated area, while Cr

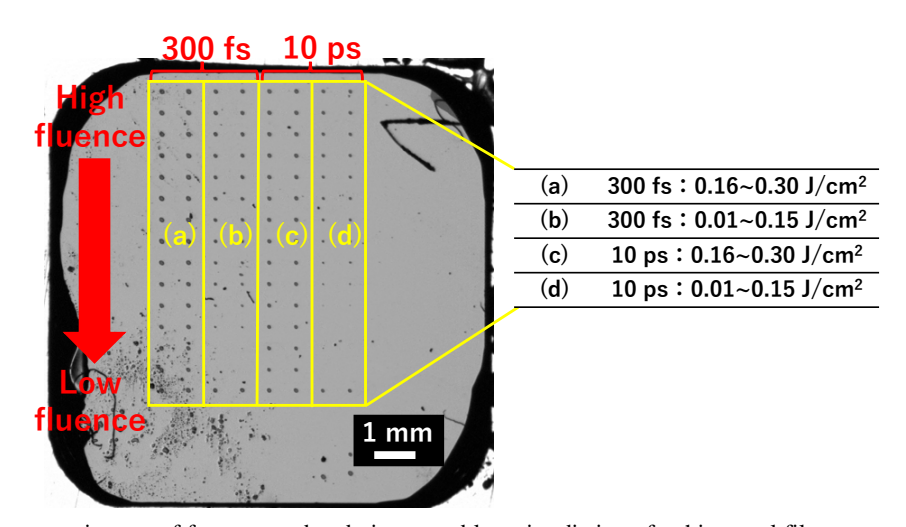
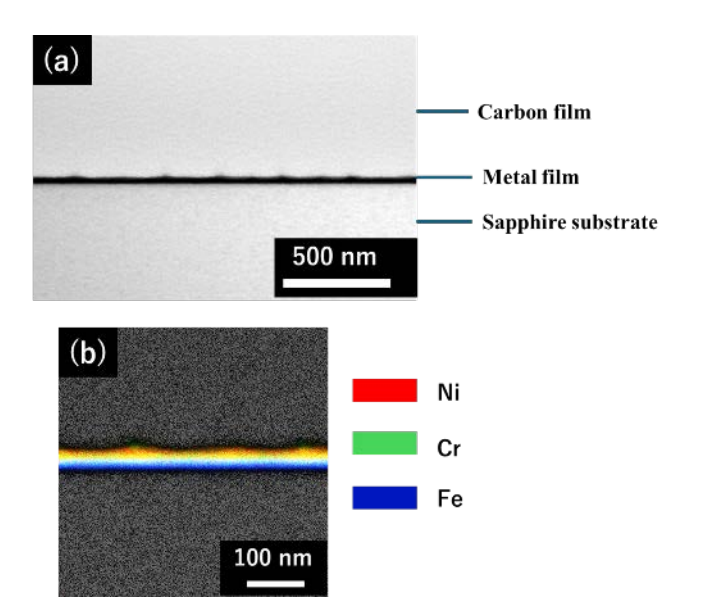


Fig. 4 Optical microscope images of femtosecond and picosecond laser irradiation of a thin metal film on sapphire. (a) Laser irradiated area with a pulse duration of 300 fs and a fluence of  $0.16 \sim 0.30 \text{ J/cm}^2$ . (b) Laser irradiated area with a pulse duration of 300 fs and a fluence of  $0.01 \sim 0.15 \text{ J/cm}^2$ . (c) Laser irradiation area with a pulse duration of 10 ps and a fluence of  $0.16 \sim 0.30 \text{ J/cm}^2$ . (d) Laser irradiation area with a pulse duration of 10 ps and a fluence of  $0.01 \sim 0.15 \text{ J/cm}^2$ .



**Fig.5** (a) STEM bright-field image of the non-laser-irradiated area. (b) Magnified EDS image of (a), with color coding for each element: Fe (blue), Cr (green), and Ni (red).

and Ni signals almost disappeared. This suggests vaporization of these elements under high fluence conditions.

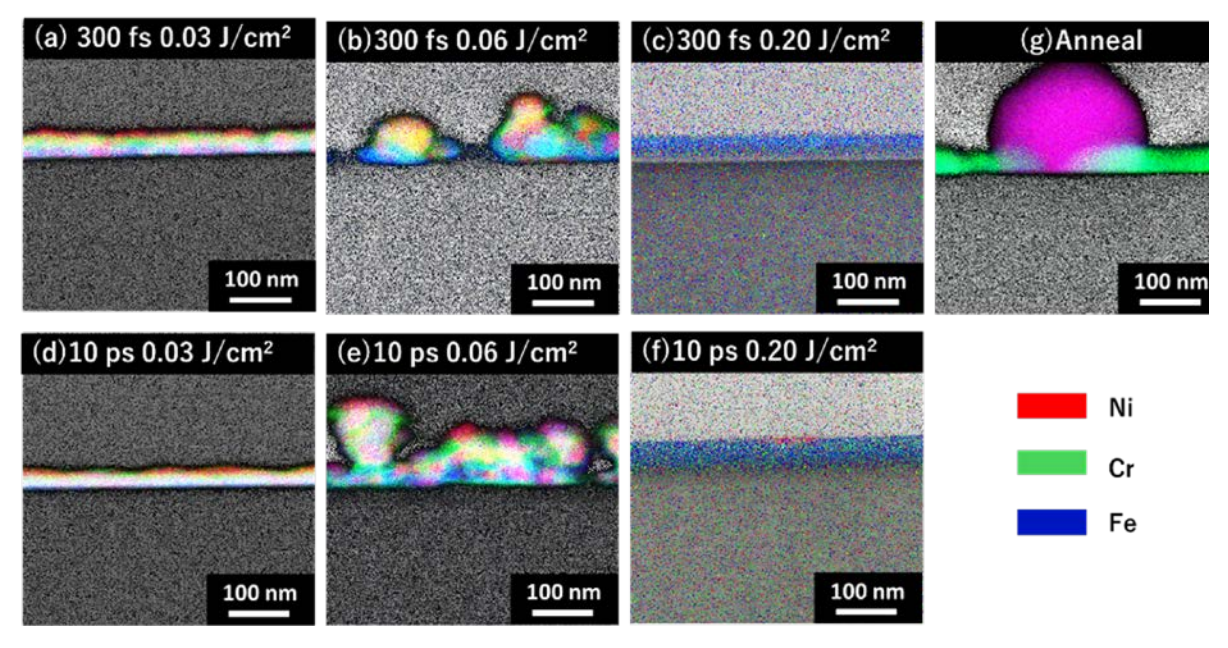
For comparison, thermal annealing was performed at 1000 °C. After annealing, the morphology of the metal film was severely disrupted. Fe and Ni formed rounded, droplet-like structures, indicative of melting and surface tension driven solidification, while Cr largely retained its original geometry. This behavior can be attributed to Cr's significantly higher melting point relative to Fe and Ni. Notably, under certain ultrashort-pulse laser conditions, the thin film morphology was better preserved than after annealing. This suggests that the rapid quenching associated with ultrashort pulsed lasers enabled re-solidification of the molten metal

before significant structural deformation could occur. These results indicate that ultrashort pulse laser irradiation, as opposed to conventional thermal annealing, can suppress elemental segregation and promote uniform alloy formation, even in multilayer metal systems.

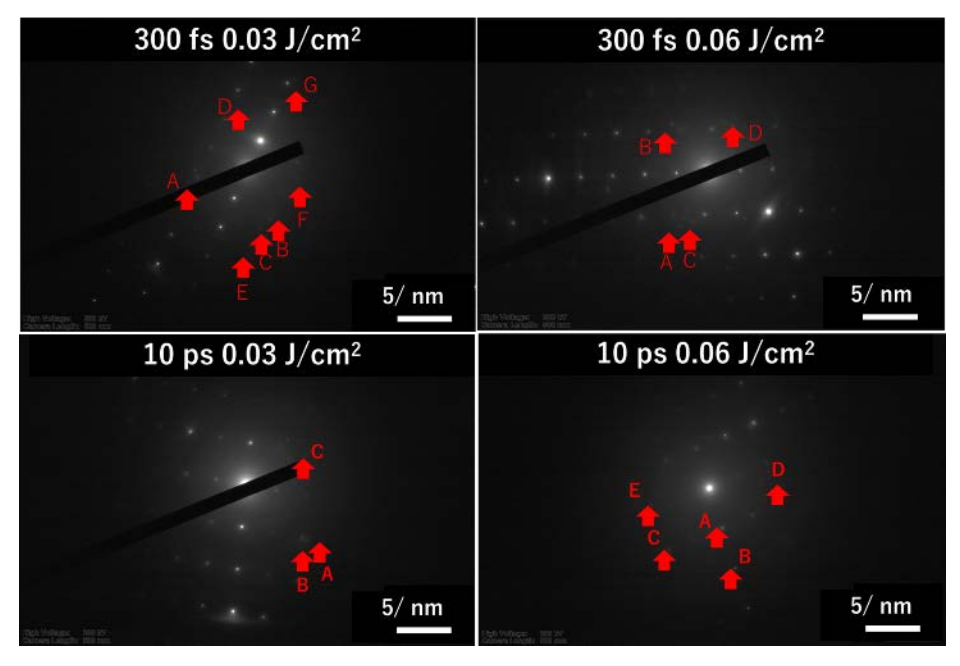
While EDS mapping provides insights into elemental distribution, it does not offer direct information on compositions. To identify the compounds generated by laser processing, SAED analysis was conducted. SAED patterns were collected from the bright regions presumed to contain a mixture of Fe, Cr, and Ni. To isolate signals from newly formed phases, diffraction spots corresponding to the substrate (sapphire) and unreacted elements (Fe, Cr, Ni) were systematically excluded. To reduce measurement errors, three d-spacing values were obtained for each region and cross-referenced using crystallographic database software (CSManager). Candidate materials were then assigned based on the best matches with measured d-values.

Figure 7 shows SAED patterns obtained at pulse durations of 300 fs and 10 ps. As summarized in Table 1, several compounds including oxides, binary alloys, and previously unreported ternary alloy were identified at a pulse duration of 300 fs. A similar trend was observed at 10 ps, with both oxide formation and alloying. Although a wide range of oxides can potentially form, the ternary alloy composed of iron, chromium, and nickel was observed for the first time under ultrashort pulsed laser irradiation. This result represents a promising step toward the fabrication of high-entropy alloys.

When an ultrashort pulsed laser irradiates a material, the resulting processes can be broadly categorized into thermal and nonthermal regimes depending on the pulse duration. The boundary between these regimes is generally considered to be on the order of picoseconds, as it is determined by the electron–phonon coupling time that is, the time required for energy transfer from free electrons to the lattice ions. For the



**Fig. 6** Energy-dispersive X-ray spectroscopy (EDS) images of laser-irradiated regions under varying irradiation conditions. (a) Region irradiated with a 300 fs pulse duration and a fluence of 0.03 J/cm². (b) Region irradiated with a 300 fs pulse duration and a fluence of 0.06 J/cm². (c) Region irradiated with a 300 fs pulse duration and a fluence of 0.20 J/cm². (d) Region irradiated with a 10 ps pulse duration and a fluence of 0.03 J/cm². (e) Region irradiated with a 10 ps pulse duration and a fluence of 0.06 J/cm². (f) Region irradiated with a 10 ps pulse duration and a fluence of 0.20 J/cm². (g) Region annealed at 1000°C for 2 minutes.



**Fig. 7** SAED patterns obtained from the regions where apparent intermixing was observed. Diffraction spots indicated by red arrows are used for the d-values analysis. (a) Region irradiated with a 300 fs pulse duration at a fluence of 0.03 J/cm². (b) Region irradiated with a 300 fs pulse duration at a fluence of 0.06 J/cm². (c) Region irradiated with a 10 ps pulse duration at a fluence of 0.03 J/cm². (d) Region irradiated with a 10 ps pulse duration at a fluence of 0.06 J/cm².

metallic elements used in this study, the electron phonon relaxation time is estimated to be in the order of a few picoseconds[15]. Therefore, a 300 fs pulse duration, being significantly shorter than the relaxation time, is expected to induce nonthermal processes, whereas a 10 ps pulse, which is comparable to relaxation time, is expected to involve intermediate behavior between thermal and nonthermal mechanisms. In this study, under 10 ps irradiation, the formation of a phase normally not observed at room temperature was confirmed. This suggests that even at a pulse duration comparable to the electron-phonon relaxation time, the generation of high temperature phases is possible. Furthermore, a greater number of equiatomic alloy candidates were identified under 300 fs pulse irradiation compared to the 10 ps condition. This implies that 300 fs pulses promote the formation of equiatomic and metastable phases more effectively,

highlighting the advantage of ultrashort laser pulses in driving non-equilibrium material processing.

Table 2 shows the results of quantitative elemental analysis conducted in the metallic thin-film regions for each laser parameter set. Under most conditions, Fe, Cr, and Ni were detected in approximately equiatomic proportions, indicating effective elemental intermixing. Notably, under the condition of 300 fs pulse duration at a fluence of 0.06 J/cm², a significant compositional deviation was observed specifically, a marked decrease in Fe content accompanied by an increase in Ni concentration. This may be attributed to damage induced in the metal thin film by laser irradiation, which could have caused elemental segregation, leading to compositional imbalance. These observations underscore the importance of optimizing laser parameters to suppress film degradation while simultaneously promoting uniform elemental mixing,

Table 1 Candidate laser-induced phases at different laser durations.

Pulse duration	Candidate phase	
300 fs	FeO <sub>3</sub> , Fe <sub>1.56</sub> O <sub>2.38</sub> , Fe <sub>0.96</sub> O <sub>2</sub> , Fe <sub>2</sub> O <sub>3</sub> , Fe <sub>3</sub> O <sub>4</sub> , Fe <sub>3.644</sub> O <sub>4</sub> , Fe <sub>3.672</sub> O <sub>4</sub> , Fe <sub>3.716</sub> O <sub>4</sub> , Fe <sub>3.728</sub> O <sub>4</sub> , Fe <sub>7.784</sub> O <sub>12</sub> , Fe <sub>10.596</sub> O <sub>4</sub> , Fe <sub>11.52</sub> O <sub>18</sub> , Fe <sub>11.744</sub> O <sub>18</sub> , Fe <sub>11.892</sub> O <sub>18</sub> , Fe <sub>11.905</sub> O <sub>18</sub> , Fe <sub>11.928</sub> O <sub>18</sub> , Fe <sub>13.6</sub> O <sub>32</sub> , Fe <sub>17</sub> O <sub>24</sub> , Fe <sub>21.16</sub> O <sub>31.92</sub> , Fe <sub>21.336</sub> O <sub>32</sub> , Fe <sub>62.92</sub> O <sub>94.8</sub> ,	
	Cr <sub>2</sub> O <sub>3</sub> , Cr <sub>17</sub> O <sub>80</sub> , NiO, NiO <sub>2</sub> , Ni <sub>3</sub> O <sub>6.6</sub> , Ni <sub>1.875</sub> O <sub>2</sub> ,	
	FeCr <sub>2</sub> O <sub>4</sub> , Fe <sub>2</sub> Cr <sub>2</sub> O <sub>5</sub> , Fe <sub>6</sub> Cr <sub>17</sub> O <sub>80</sub> , FeNi <sub>2</sub> O <sub>4</sub> , Fe <sub>6</sub> Ni <sub>1.875</sub> O <sub>2</sub> , FeNiO <sub>8</sub> , Fe <sub>13.6</sub> Ni <sub>11.44</sub> O <sub>32</sub> , CrNiO <sub>4</sub> , CrNiO <sub>4</sub> , Cr <sub>2</sub> NiO <sub>4</sub> ,	
	FeNi, FeNi <sub>3</sub> , Fe <sub>2.03</sub> Ni <sub>1.97</sub> , CrNi, CrNi <sub>3</sub> , Cr <sub>1.6</sub> Ni <sub>2.4</sub> , Fe <sub>0.45</sub> Cr <sub>0.18</sub> Ni <sub>0.37</sub>	
10 ps	Fe <sub>2</sub> O <sub>3</sub> , Fe <sub>3</sub> O <sub>4</sub> , Fe <sub>4</sub> O <sub>5</sub> , Fe <sub>0.96</sub> O <sub>2</sub> , Fe <sub>1.56</sub> O <sub>2.38</sub> , Fe <sub>3.644</sub> O <sub>4</sub> , Fe <sub>7.784</sub> O <sub>12</sub> , Fe <sub>9.56</sub> O <sub>22</sub> , Fe <sub>9.74</sub> O <sub>22</sub> Fe <sub>9.86</sub> O <sub>16</sub> , Fe <sub>10.596</sub> O <sub>4</sub> , Fe <sub>11.52</sub> O <sub>18</sub> , Fe <sub>11.744</sub> O <sub>18</sub> , Fe <sub>11.892</sub> O <sub>18</sub> , Fe <sub>11.905</sub> O <sub>18</sub> , Fe <sub>11.928</sub> O <sub>18</sub> , Fe <sub>13.6</sub> O <sub>32</sub> , Fe <sub>21.16</sub> O <sub>31.92</sub> , Fe <sub>21.336</sub> O <sub>32</sub> , Fe <sub>62.92</sub> O <sub>94.8</sub> ,	
	Cr <sub>2</sub> O <sub>3</sub> , NiO, NiO <sub>2</sub> ,	
	FeCr <sub>2</sub> O <sub>4</sub> , Fe <sub>2</sub> Cr <sub>2</sub> O <sub>5</sub> , Fe <sub>6</sub> Cr <sub>17</sub> O <sub>80</sub> , Fe <sub>13.6</sub> Ni <sub>11.44</sub> O <sub>32</sub> , FeNiO <sub>8</sub> , Cr <sub>2</sub> NiO <sub>4</sub> , CrNiO <sub>4</sub> ,	
	FeCr, Fe <sub>1.6</sub> Cr <sub>0.4</sub> , Fe <sub>0.6</sub> Cr <sub>1.4</sub> , Cr <sub>1.6</sub> Ni <sub>2.4</sub> , Fe <sub>2.03</sub> Ni <sub>1.97</sub> , Fe <sub>0.45</sub> Cr <sub>0.18</sub> Ni <sub>0.37</sub>	

Table 2 Compositional variations of Fe, Cr, and Ni as a function of laser pulse duration and fluence.

Laser parameters	Fe(at.%)	Cr(at.%)	Ni(at.%)
300 fs 0.03 J/cm <sup>2</sup>	15.3	17.2	13.0
$300 \text{ fs } 0.06 \text{ J/cm}^2$	4.00	8.9	16.3
$10 \text{ ps } 0.03 \text{ J/cm}^2$	21.0	22.2	21.6
10 ps 0.06 J/cm <sup>2</sup>	7.8	9.3	10.4

which is essential for the formation of equiatomic ternary alloys.

To date, both binary and ternary alloy systems have been successfully synthesized. In future work, we aim to increase the number of constituent elements, ultimately targeting the development of high-entropy alloys.

## 4. Conclusion

In this study, thin films of Fe, Cr, and Ni were sequentially deposited on a sapphire substrate and subjected to ultrashort pulsed laser irradiation. EDS analysis revealed that, at low fluence and constant pulse duration, alloy formation occurred while preserving the original morphology of the metallic film. As the laser fluence increased, the film structure became increasingly disrupted, and homogeneous mixing of all three elements was no longer observed. In contrast, conventional thermal annealing resulted in significant morphological changes, including the formation of droplet-like features, particularly for Fe and Ni. This behavior is attributed to melting due to prolonged heating and solidification due to surface tension. Compared to annealing, ultrashort pulsed laser irradiation induced melting and subsequent solidification within a significantly shorter time frame. These findings suggest that ultrashort pulsed laser processing is more effective than annealing in suppressing elemental segregation and facilitating the formation of high quality alloys. Furthermore, SAED analysis indicated the potential formation of ternary alloy that has not been previously reported. Even at 10 ps, which corresponds to the collision relaxation time, the formation of the high temperature phase was observed.

Results from quantitative analysis indicate that, under high fluence, the metal thin film undergoes structural damage and exhibits elemental segregation, underscoring the necessity of optimizing laser parameters to achieve homogeneous elemental distribution.

SAED analysis showed that the sample irradiated with the 300 fs pulse showed a slightly higher number of unoxidized, equal ratio alloy candidates.

This suggests that the shorter pulse duration of 300 fs may have led to more rapid quenching, which potentially suppressed elemental segregation more effectively than the 10 ps condition.

## Acknowledgments

This work was partially supported by THE AMADA FOUNDATION (AF-2020201-A3), the Amano Institute of Technology, Power Academy, Iketani Science and Technology Foundation, and Nippon Sheet Glass Faundation for Materials Science and Engineering.

This work was performed using facilities of the Institute for Solid State Physics, the University of Tokyo(ISSPkyodo-202311-GNBXX-0005)

#### References

- [1] B. Cantor, I. T. H. Chang, P. Knight, and A. J. B Vinc ent: Mater. Sci. Eng. A., 375, (2004) 213.
- [2] J. W. Yeh, S. K. Chen, S. J. Lin, J. Y. Gan, T. S. Chin, T. T. Shun, C. H. Tsau, and S. Y. Chang: Adv. EngMater., 6, (2004) 299.
- [3] P. Ren, G. Yang, Y. Jin, C. Peng, X. Lei, F. Yin, Z. Zhao, Y. Wang, Z. Guo, Z. Chen, and F. Re: J. Alloya Compd., 1024, (2025) 180153.
- [4] S. Aravind Krishna, N.Noble, N.Radhika, and B. Saleh: J. Manuf. Process., 109, (2024) 583.
- [5] B. Yu, Y. Ren, Y. Zeng, W. Ma, K. Morita, S. Zhan. Y. Lei, G. Lv, S. Li, and J. Wu: J. Mater. Res. Technol., 29, (2024) 2689.
- [6] D. Redka, C. Gadelmeier, J. Winter, M. Spellauge, C. Eulenkamp, P. Calta, U. Glatzel, J. Mińar, and H. P. Huber: Appl. Surf. Sci., 544, (2021) 148839.
- [7] M. Todai, T. Nagase, T. Hori, A. Matsugaki, A. Sekita, and T. Nakano: Scr. Mater., 129, (2017) 65.
- [8] B. Zhang, J. Chen, and C. Coddet: J. Mater. Sci. Technol., 29, (2023) 863.
- [9] T. DebRoy, H. L. Wei, J. S. Zuback, T.Mukherjee, J.W. Elmer, J.O. Milewski, A.M. Beese, A. Wilson-Heid, A. De, and W. Zhang: Prog Mater Sci., 92, (2018) 112.
- [10] O. Gokcekaya, T. Ishimoto, Y. Nishikawa, Y. S. Kim, A. Matsugaki, R. Ozasa, M. Weinmann, C. Schnitter, M. Stenzel, H. S. Kim, Y. Miyabayashi, and T. Nakano: Mater. Res. Lett., 11, (2022) 274.
- [11] D.S Ivanov ,Z. Lin, B. Rethfeld,G. M. O'Connor, T. J. Glyn, and L. V. Zhigilei: J. Appl. Phys., 107, (2010) 013519
- [12] T. Okada, T. Tomita, H. Katayama, Y. Fuchikami, T. Ueki, H. Hisazawa, and Y. Tanaka: Appl. Phys. A., 125, (2019) 690.
- [13] T. Furuichi, H. Seki, T. Kawano, K. Takabayashi, T. Endo, E. Tsuchiya, M. Yamaguchi, Y. Kobayashi, T. Okada, and T. Tomita: Appl. Phys. A., 130, (2024) 818.
- [14] T.Tomita, T.Kawano, K. Nakagawa, H. Seki, K. Takabayashi, T. Endo, E. Tsuchiya, M. Yamaguchi, Y. Kobayashi, and T. Okada: In preparation.
- [15] S. I. Anisimov, and B. Rethfeld: Proc. SPIE, Vol. 3093, (1997) 192

(Received: June 25, 2025, Accepted; November 3, 2025)